

# Symmetry Breaking and Spatiotemporal Pattern Formation in Photonic Time Crystals

Egor I. Kiselev<sup>1,2</sup> and Yiming Pan<sup>3</sup>

<sup>1</sup>*Physics Department, Technion, 320003 Haifa, Israel*

<sup>2</sup>*The Helen Diller Quantum Center, Technion, Haifa 3200003, Israel \**

<sup>3</sup>*School of Physical Science and Technology and Center for Transformative Science, ShanghaiTech University, Shanghai 200031, China*

In this work, we explore the dynamics of time varying photonic media with an optical Kerr nonlinearity and an associated phase transition. The interplay between a periodically modulated permittivity and the nonlinearity induces a continuous transition of electromagnetic waves to a state with broken spatial and time translation symmetries. This transition gives rise to a lattice-like wave pattern, in many ways similar to a spatial crystallization in solids. Symmetry breaking triggers the emergence of soft, Goldstone-like modes, which propagate as deformations of the lattice structure, as well as massive Higgs-like modes – spatially uniform oscillations of the field amplitude. We extend the analysis of the non-equilibrium symmetry breaking to 2+1 dimensional time varying media and discuss pattern formation as well as the connection to discrete time crystals.

## I. INTRODUCTION

The propagation of electromagnetic fields through media with time varying material parameters has been considered early on [1–3]. More recently, time varying media have attracted attention in photonics [4], metamaterials [5, 6], and material science [7], particularly in the field of epsilon near zero materials [8–11]. They are viewed as promising candidates for realizing such effects as momentum-gapped (k-gapped) states, nonreciprocity [12], time switching [13], time-varying mirrors [11], lasing and amplification [14]. From a fundamental perspective, the non-trivial statistical properties of randomly driven time-varying media [15], their topological [16] and radiative [17, 18] properties have been explored. Beyond optics, hydrodynamic [19, 20] and acoustic [21] time varying systems have been studied.

In this paper, we study nonlinear photonic time crystals (nonlinear PTCs) – dielectric media with a periodically modulated permittivity [22, 23]. It is crucial to distinguish PTCs from “time crystals” in the sense of Wilczek [24–28]. While it is important to maintain this distinction, we demonstrate that, in the presence of a Kerr term, a PTC evolves to a subharmonic steady state oscillating at half the driving frequency, and thus breaks the discrete time translation symmetry of the drive on long timescales. The steady state is very much akin to Faraday waves [29–31], which are in many ways similar to classical discrete time crystals [28, 32, 33].

One of the most striking features of PTCs is the so called momentum gap (sometimes referred to as k-gap or q-gap, see Fig. 1a) – an interval of wavenumbers in which the real part of the dispersion  $\omega(q)$  becomes flat and the imaginary part changes sign, leading to exponentially growing modes inside the gap [22]. In nonlinear PTCs and time varying media, the k-gap can lead

to intriguing effects such as the formation of superluminal solitons [34–37]. We show that in PTCs featuring a generic Kerr nonlinearity, this growth heralds an instability, leading to the emergence of non-equilibrium, symmetry breaking steady-states: When the PTC’s permittivity is modulated at a frequency  $2\Omega$ , the field adopts a standing wave lattice pattern whose wavenumber  $q^*$  and lattice constant  $\lambda = 2\pi/q^*$  are determined by the condition for parametric resonance  $q^* = \Omega/c$  (Fig. 1).

Furthermore, we show that in the symmetry breaking state, slow, long-wavelength electromagnetic fields propagate through the PTC as distortions of the lattice, locally contracting or expanding the lattice constant  $\lambda$  (see Fig. 2). This behavior is reminiscent of phonons in a crystal lattice, and the corresponding distortions can be thought of as the Goldstone modes of the symmetry broken state. Additionally, the symmetry broken state hosts spatially uniform oscillations of the field amplitude at a characteristic frequency that depends on the driving strength (see Fig. 2b). These oscillations are gapped, massive modes that resemble, e.g., the Higgs modes of a superconductor.

## II. RESULTS

### Symmetry breaking transition.

In this paragraph, we investigate the symmetry breaking transition of nonlinear PTCs. We show that the transition is continuous when the modulation strength of the dielectric constant exceeds a threshold value determined by the damping.

The propagation of electromagnetic fields in a non-magnetic, isotropic, one-dimensional PTC with a generic, repulsive Kerr-nonlinearity is described by the equation [36]

$$\frac{1}{c^2} \frac{\partial^2 D}{\partial t^2} + \frac{\gamma}{c^2} \frac{\partial D}{\partial t} - (1 + h \cos 2\Omega t) \frac{\partial^2 D}{\partial x^2} = \beta |D|^2 \frac{\partial^2 D}{\partial x^2}, \quad (1)$$

\* kiselev.physics@gmail.com

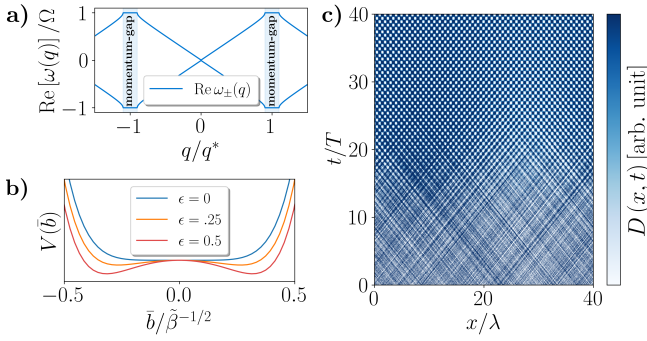


Figure 1. **a)** Real part of the dispersion relation  $\omega(q)$  of the PTC with momentum gaps at  $q^* = \Omega/c$ , where  $2\Omega$  is the modulation frequency of the dielectric constant. **b)** Effective potential  $V(\bar{b})$  for the displacement field amplitude  $\bar{b}$  with minima corresponding to steady states with broken translational and discrete time translational symmetries (see Eq. (9)). Here,  $\epsilon$  is a parameter that encodes the relative strength of the modulation of the dielectric constant with respect to damping (see Eq. (5)). **c)** A numerical simulation of Eq. (1) showing the self organization of electric fields into the symmetry breaking steady state, corresponding to a minimum of the potential  $V(\bar{b})$ . To produce the plot, we choose a modulation strength close to the threshold yielding  $\epsilon \approx 0.02$ . The  $t$ - and  $x$ -axes are drawn in units of  $T = 2\pi/\Omega$  and  $\lambda = 2\pi/q^*$ .

where  $D(x, t)$  is the displacement field,  $\gamma$  is the decay rate of the electromagnetic field,  $c$  is the speed of light and  $h$  is a dimensionless parameter controlling the modulation strength of the dielectric constant. In what follows we assume  $h > 0$ . For brevity, we omit vector signs. For a small  $h \ll 1$ , an approximate solution to Eq. (1) can be found with the slowly varying envelope approximation. Anticipating that the time dependent term will lead to a parametric response at half the modulation frequency  $\Omega$  [38], we choose the ansatz

$$D = a(t) \cos(\Omega t) \cos(q^* x) + b(t) \sin(\Omega t) \cos(q^* x). \quad (2)$$

Here  $q^*$  is a critical wavenumber determined by the condition

$$\Omega = c|q^*|. \quad (3)$$

To first order in  $h$ , and projecting the nonlinear term of Eq. (1) onto the ansatz of Eq. (2), i.e. disregarding harmonics oscillating at frequencies  $\pm 3\Omega$  and faster, we obtain

$$\begin{aligned} \dot{a} &= -\frac{\gamma}{2}a - \tilde{h}\Omega b + \tilde{\beta}\Omega b(a^2 + b^2) \\ \dot{b} &= -\frac{\gamma}{2}b - \tilde{h}\Omega a - \tilde{\beta}\Omega a(a^2 + b^2), \end{aligned} \quad (4)$$

with  $\tilde{h} = h/4$  and  $\tilde{\beta} = 9\beta/32$ .

We deduce from the amplitude equations (4) that for  $h < h_c$ , where

$$h_c = 2\gamma/\Omega,$$

the PTC is stable around the trivial fixed point  $D(x, t) = 0$ . For  $h > h_c$  this fixed point becomes unstable, leading an initially exponential growth of the amplitudes  $a, b$ . The nonlinear terms then become increasingly important, and force the amplitudes to saturate. Eventually, the PTC reaches a new fixed point, which corresponds to the symmetry breaking phase that we want to study.

It is useful to consider two distinct regimes. In the first regime, which we will call this the *near-critical regime*,  $h$  is close to the critical threshold value  $h_c$ . In this case, both, the transition speed and the amplitudes  $a, b$  at the fixed point are determined by the small parameter

$$\epsilon = \frac{h - h_c}{h_c}. \quad (5)$$

In the second regime,  $h \gg h_c$  holds. Here, the damping can be disregarded to a good approximation. Let us term this the *weakly-damped regime*. With  $\gamma$  set to zero, the equations (4) can be derived from the Hamiltonian

$$H(a, b) = \frac{\tilde{h}\Omega}{2}(a^2 - b^2) + \frac{\tilde{\beta}\Omega}{4}(a^4 + b^4) + \frac{\tilde{\beta}\Omega}{2}a^2b^2. \quad (6)$$

Formally, we can think of  $a$  as a momentum variable and  $b$  as a coordinate. The phase profile corresponding to  $H(a, b)$  and the trajectories of  $a$  and  $b$  during the symmetry breaking phase transition are shown in Fig. 2c. The minima of the Hamiltonian (6) are the stable fixed points of Eqs. (4), and are located at

$$a_0 = 0, \quad b_0 = \pm \sqrt{\frac{\tilde{h}}{\tilde{\beta}}}. \quad (7)$$

For a small damping  $\gamma \ll h\Omega$ , the solutions (7) are slightly modified. To first order in  $\gamma/h\Omega$ , we find  $a_0 \approx \mp \frac{\gamma}{\Omega\sqrt{8\tilde{\beta}h}}$  and  $b_0 \approx \pm \sqrt{\frac{\tilde{h}}{\tilde{\beta}}} \mp \frac{\gamma^2}{16\Omega^2\sqrt{\tilde{\beta}h}}$ . For the most part (except when studying the transition to the symmetry breaking state), we will not be interested in the damping, and only include it for the sake of numerical stability. For weak damping, the system will evolve to a state described by the above solution, and the  $D$ -field will be given by

$$D_0(x, t) = a_0 \cos(\Omega t) \cos(q^* x) + b_0 \sin(\Omega t) \cos(q^* x). \quad (8)$$

This steady state of the nonlinear PTC breaks the continuous spatial translation, and the discrete time translation symmetries of Eq. (1). The latter follows from the fact that the solution  $D_0(x, t)$  of Eq. (8) is, unlike Eq. (1) not invariant under the time translation  $t \rightarrow t + \frac{\pi}{\Omega}$ .

Let us now turn to the weakly damped regime where the modulation strength  $h$  is close to the instability threshold  $h_c$ . This regime is useful to study the transition dynamics from the trivial to the symmetry breaking state. In particular, it can be shown that the transition into the symmetry breaking steady state is a continuous phase transition. To this purpose, we rewrite the

amplitude equations for  $a(t)$ ,  $b(t)$  in terms of the new variables  $\bar{a}(t) = a(t) + b(t)$ ,  $\bar{b}(t) = a(t) - b(t)$ . A perturbative expansion of Eqs. (4) in the small parameter  $\epsilon$  of Eq. (5) (see supplement) then predicts that the transitional dynamics can be described by a gradient descent equation for  $\bar{b}(t)$ :

$$\dot{\bar{b}} = -\frac{\partial V(\bar{b})}{\partial \bar{b}},$$

where  $V(\bar{b})$  is an effective double-well potential:

$$V(\bar{b}) = -\epsilon \frac{\tilde{h}_c \Omega}{2} \bar{b}^2 + \frac{\tilde{\beta}^2 \Omega}{48 \tilde{h}_c} \bar{b}^6. \quad (9)$$

We plot the effective potential for different  $\epsilon$  in Fig. 1b and conclude that the transition into the symmetry breaking state is continuous, i.e. the system goes through a soft bifurcation when  $h$  reaches the critical driving strength  $h_c$ . In terms of the original  $a$  and  $b$ , the potential minima (and approximate fixed points of Eqs. (4)) are located at

$$a_0 = -b_0 = \pm \sqrt{\frac{\tilde{h}_c}{\tilde{\beta}}} (2\epsilon)^{1/4}. \quad (10)$$

The result of a numerical simulation of Eq. (1) for  $\epsilon = 0.005$  is depicted in Fig. 1c, showing how the displacement field inside the PTC begins to self-organize itself into the standing wave pattern predicted in Eqs. (2) and (10). All simulations in this paper were carried out using the Dedalus software package [39].

### Emergent collective modes.

In the previous section, we demonstrated that the unstable, exponentially growing modes of a nonlinear PTC herald the onset of a new phase. After a short transitional period, the nonlinear PTC enters a steady state with broken spatial translation and discrete time translation symmetries. In this section, we focus on small fluctuations around this new state. We demonstrate that the lattice structure of the electric field supports soft, wavelike excitations, which propagate through the lattice, similar to phonons in a crystal lattice. These excitations are Goldstone-like modes that stem from the breaking of the continuous spatial translation symmetry. Additionally, the steady state exhibits a gapped mode, which is absent in the symmetric state.

These effects are most pronounced in the *weakly damped regime*, where  $h \gg h_c$ , to which we will stick for the rest of this discussion. We begin with the soft modes. Note that the phase of the spatial part of the standing wave in Eq. (8) is chosen spontaneously. Replacing  $x \rightarrow x + \phi/q^*$  in Eq. (8), we obtain another valid solution to Eq. (1). Following the usual logic of the Goldstone theorem [40], we expect that, since a

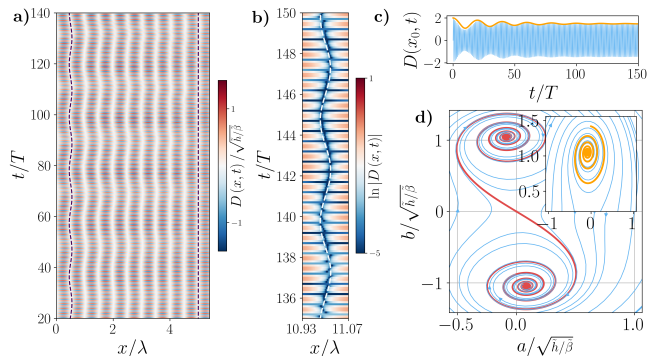


Figure 2. **a)** Goldstone-like distortions propagating through the electric field lattice of the PTC in the symmetry broken state. The displacement field is given by  $D(x, t) = \sqrt{\tilde{h}/\tilde{\beta}} \sin(\Omega t) \cos(q^* x + \phi(x, t))$ . An oscillatory boundary condition of the form  $\phi(x=0, t) = -0.3 \sin(\omega_G(Q)t)$  is applied. The propagation of the phase  $\phi(x, t)$  through the wave-lattice is described by Eq. (11). The dashed black curves show the nodes of the standing wave D-field, described by  $q^* x + \phi(x, t) = \pi/2$ . **b)** A Goldstone-like mode as observed starting with an initial condition  $D(x) = \sqrt{\tilde{h}/\tilde{\beta}} \cos(q^* x - 0.2 \sin(q^* x/5))$  at  $t=0$ . The Goldstone-like mode propagates according to Eq. (11) (white dashed line), where small damping  $\gamma = 0.0016\omega$  was taken into account. **c)** The Higgs-like amplitude mode derived in Eq. (13) is depicted. The numerical solution (blue), is plotted against the amplitude envelope predicted in Eq. (13). The amplitude trajectory corresponding to the amplitude oscillation is shown in the inset of subfigure d) **d)** Phase profiles of the amplitude Hamiltonian (6). The red curves indicate the two possible amplitude trajectories  $a(t)$ ,  $b(t)$  during the phase transition. The inset shows the trajectory corresponding to the damped Higgs-like oscillation of subfigure b).

uniform offset  $\phi$  is inconsequential for the system's dynamics, a long-wavelength spatial dependence of  $\phi$  will only have a small impact on the time evolution. It remains to show that a long-wavelength perturbation of the form  $\phi(x, t_0) = \phi_Q e^{iQx}$ , where  $Q \ll q^*$ , will propagate through the system as a wave with frequency  $\omega_G(Q)$ , and that  $\omega_G(Q) \rightarrow 0$ , as  $Q \rightarrow 0$ , i.e. the dispersion  $\omega_G(Q)$  is soft. Indeed, we find that this is true (see Supplement): For  $|\phi| \ll 1$ , the propagation of the Goldstone-like mode is described by the equation

$$\frac{1}{c^2} \frac{\partial^2 \phi}{\partial t^2} = \left(1 - \frac{1}{3}h\right) \frac{\partial^2 \phi}{\partial x^2}. \quad (11)$$

The dispersion of the mode is  $\omega_G(Q) = c_G Q$ , where  $c_G = \sqrt{1 - h/3}c$ . Fig. 2a shows the numerical simulation of Eq. (1), where a boundary condition of the form  $\phi(x=0, t) = -0.3 \sin(\omega_G(Q)t)$  was applied. The perturbation at the boundary propagates as a Goldstone-like mode whose dynamics is described by Eq. (11), and forms a standing wave, such that the phase throughout the PTC is given by  $\phi(t, x) = [\sin(\omega_G(Q)t - Qx) + \sin(\omega_G(Q)t + Qx)]/2$ . For the

simulation, we chose  $Q = 2\pi/\Lambda$ , where  $\Lambda = 20\lambda$  and  $\lambda = 2\pi/q^*$ . We also demonstrate the propagation of the Goldstone-like mode starting from an initial field  $D(x) = \sqrt{\tilde{h}/\tilde{\beta}} \cos(q^*x - 0.2 \sin(q^*x/5))$  at  $t = 0$ . The propagation of the distortion for long times is shown in Fig. 2b.

In addition to the soft Goldstone mode, the steady-state of Eq. (8) supports spatially uniform oscillations of the amplitudes  $a$  and  $b$  around the minima of Eq. (7). This amplitude oscillation can be viewed as a massive Higgs mode. To derive the oscillation frequency, we expand the effective Hamiltonian (6) around these minima:

$$H \approx -\frac{\tilde{h}^2\Omega}{4\tilde{\beta}} + \tilde{h}\Omega(\delta b^2 + \delta a^2). \quad (12)$$

Hamilton's equations read

$$\begin{aligned} \delta\dot{b} &= 2\tilde{h}\Omega\delta a \\ \delta\dot{a} &= -2\tilde{h}\Omega\delta b. \end{aligned} \quad (13)$$

Solving for  $a(t)$ , we find  $\delta\ddot{a} + (2\tilde{h}\Omega)^2\delta a = 0$ . Thus, the PTC supports uniform amplitude oscillations of frequency  $2\tilde{h}\Omega$ . For finite  $\gamma$ , the above equations (13) will obtain a damping term and read  $\delta\dot{b} = -\gamma b/2 + 2\tilde{h}\Omega\delta a$ ,  $\delta\dot{a} = -\gamma a/2 - 2\tilde{h}\Omega\delta b$ . The solution of these equations (including damping) is shown in Fig. 2b together with the field amplitude  $D(t, 2\pi/q^*)$ . We point out that if no dissipative term is included in Eq. (1), the PTC, starting with an initial field distribution, will not converge to a fixed point. Instead, the amplitudes  $a, b$  will follow the Hamiltonian dynamics of Eqs. (13).

### Symmetry breaking and pattern formation in two dimensions.

So far we have considered a one-dimensional PTC. A similar symmetry breaking transition can be observed in higher dimensions. Here, the spatial second derivative in Eq. (1) is replaced by a laplacian:  $\partial^2 D/\partial x^2 \rightarrow \nabla^2 D$ . Focusing on the isotropic case, we omit vector signs. The analytical calculation presented so far can be extended to higher dimensions. There is, however, a crucial difference to consider. In one spatial dimension, the only wavenumbers for which the resonance condition (3) is fulfilled are  $\pm q^*$ . Plane waves with these two wavenumbers arrange themselves in a standing wave pattern as shown in Fig 1c. In two dimensions, all wavevectors lying on a circle of radius  $q^* = \Omega/c$  around the origin are resonant. From studies of Faraday waves, it is known that parametrically excited waves often arrange themselves in stripes, square patterns or hexagonal patterns. These arrangements correspond to one, two or three critical wavevectors  $\mathbf{q}^*$  that are chosen spontaneously during the transition to the symmetry breaking state [41, 42].

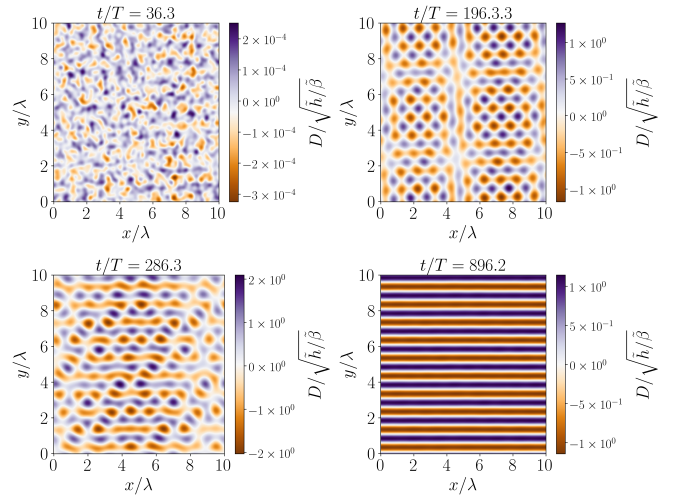


Figure 3. In two dimensions, nonlinear PTCs evolve to a stripe state that breaks the translational and rotational symmetries of the system. The figure shows the simulation of two-dimensional non-linear PTC starting from random initial conditions on square domain with commensurate periodic boundary conditions. First, the system develops inhomogeneities whose length scale is given by the critical  $q^*$ . Finally, a two dimensional stripe pattern, as predicted in Eq. (15), appears (see supplement for detailed figures).

For the simple nonlinearity of Eq. (1), we expect a stripe-pattern [41] similar to the one-dimensional scenario. On an infinite domain, the direction of  $\mathbf{q}^*$  will be chosen spontaneously. To show that the wavepattern for a two dimensional PTC is indeed a stripe arrangement, we extend the ansatz (2) to  $N$  wavevectors  $\mathbf{q}_i^*$  with a relative angle  $\theta_N$ , such that  $\mathbf{q}_i \cdot \mathbf{q}_{i+1} = \mathbf{q}_N \cdot \mathbf{q}_1 = q^{*2} \cos \theta_N$  with  $\theta_N = \pi/N$ . The driving term in Eq. (1) does not supply any momentum to the system. Therefore, each mode with a wavevector  $\mathbf{q}_i^*$  must be balanced by a mode with  $-\mathbf{q}_i^*$ . Finally, we assume that all modes share the same time dependent amplitude. Summing up, our ansatz is

$$D = (a(t) \cos(\Omega t) + b(t) \sin(\Omega t)) \sum_{i=1}^N \cos(\mathbf{q}_i^* \cdot \mathbf{x}). \quad (14)$$

When inserting this ansatz into Eq. (1), the linear terms can be treated similarly as in the 1D case. The nonlinear term, however, requires additional care. As in the 1D case, we project the nonlinear part onto the  $N$  resonant modes of the ansatz (14) and ignore fast oscillating, off-resonant terms. The equations of motion for the amplitudes  $a$  and  $b$  are similar to Eqs. (4) where  $\beta$  has to be replaced by  $\tilde{\beta}_N = 9\beta(2N-1)/32$ . Consequently, we have to make the same replacement  $\tilde{\beta} \rightarrow \tilde{\beta}_N$  in the potential (9). The new potential has minima at  $a_N = -b_N = \pm \sqrt{\tilde{h}_c/\tilde{\beta}_N} (2\epsilon)^{1/4}$ . The depth of these min-

ima depends on the number of modes  $N$ :

$$V(\bar{b}_N = a_N - b_N) \sim \frac{1}{\tilde{\beta}_N} \sim \frac{1}{2N-1}. \quad (15)$$

A similar conclusion can be reached in the weakly damped regime of Eq. (6). The depth of the minima of the Hamiltonian again behaves as  $\sim 1/\tilde{\beta}_N$ . For more complex nonlinearities containing a richer structure of spatial derivatives, the dependence of the nonlinear term on the angle  $\theta$  can compensate for the tendency of shallower minima for higher  $N$ . Typically  $\theta = \pi/2$ , or  $\theta = \pi/3$  is favored, leading to square, or hexagonal wave-lattices. In general, one expects that the system converges to the deepest minimum – in our case, to the  $N = 1$  minimum, leaving us with a single standing wave. The orientation and phase are chosen spontaneously.

Finally, we test our prediction of a stripe-pattern for the field amplitude in the symmetry broken state by performing a simulation. Starting from infinitesimal random noise on a square domain of size  $10\lambda$  with periodic boundary conditions, we let the system evolve in time and track the field amplitude. The results for the near critical case with  $\epsilon = 0.3$  are shown in Fig. 3. Interestingly, before the PTC reaches the final stripe state, it goes through a series of nearly-periodic patterns, which can be stable for many (up to hundreds) oscillation periods.

### III. DISCUSSION

Summing up, we investigated the long term behavior of a photonic time crystal with a generic Kerr nonlinearity. We have shown that the initially exponential

growth of unstable gap modes in these systems heralds the transition to a new symmetry breaking steady state. In this state, the field configuration is a standing wave lattice, where the lattice spacing is determined by the resonant wavenumber  $q^*$ , fulfilling the resonance condition  $\Omega = cq^*$ . The breaking of continuous spatial translation symmetry is accompanied by the appearance of soft Goldstone-like modes, which consist of propagating, wavelike lattice distortions, similar to phonons in a crystal lattice. In addition, gapped modes that correspond to amplitude oscillations of the electric field emerge. The dispersions of these emergent modes depend on the driving strength, which opens the possibility to use nonlinear PTCs in the symmetry broken state as tunable metamaterials. We also investigated the behavior of nonlinear PTCs in two spatial dimensions, and showed that the electric fields self-organize to stripe patterns that break the translational, and rotational symmetries of the system. This behavior could help to create controllable, spatially structured high intensity electric fields.

Furthermore, the predicted steady state exhibits subharmonic response, and breaks the discrete time translation symmetry of the periodic modulation. This is a common feature of many types of parametrically driven nonlinear waves [31, 43], as it has been pointed out in recent literature on time crystals [28, 32, 33]. Thus the nonlinear PTC exhibits discrete time crystalline behavior in the sense of a phase of matter [28].

### ACKNOWLEDGMENTS

We thank S. Gomé and M. Segev for useful discussions. E.K. acknowledges financial support by the Helen Diller quantum center.

- 
- [1] F. R. Morgenthaler, Velocity modulation of electromagnetic waves, IRE Transactions on microwave theory and techniques **6**, 167 (1958).
  - [2] D. Holberg and K. Kunz, Parametric properties of fields in a slab of time-varying permittivity, IEEE Transactions on Antennas and Propagation **14**, 183 (1966).
  - [3] L. Felsen and G. Whitman, Wave propagation in time-varying media, IEEE Transactions on Antennas and Propagation **18**, 242 (1970).
  - [4] E. Galiffi, R. Tirole, S. Yin, H. Li, S. Vezzoli, P. A. Huidobro, M. G. Silveirinha, R. Sapienza, A. Alú, and J. Pendry, Photonics of time-varying media, Advanced Photonics **4**, 014002 (2022).
  - [5] X. Wang, M. S. Mirmoosa, V. S. Asadchy, C. Rockstuhl, S. Fan, and S. A. Tretyakov, Metasurface-based realization of photonic time crystals, Science Advances **9**, eadg7541 (2023).
  - [6] T. T. Koutserimpas and C. Valagiannopoulos, Multi-harmonic resonances of coupled time-modulated resistive metasurfaces, Physical Review Applied **19**, 064072 (2023).
  - [7] S. Saha, O. Segal, C. Fruhling, E. Lustig, M. Segev, A. Boltasseva, and V. M. Shalaev, Photonic time crystals: a materials perspective, Optics Express **31**, 8267 (2023).
  - [8] Y. Zhou, M. Z. Alam, M. Karimi, J. Upham, O. Reshef, C. Liu, A. E. Willner, and R. W. Boyd, Broadband frequency translation through time refraction in an epsilon-near-zero material, Nature communications **11**, 2180 (2020).
  - [9] V. Bruno, S. Vezzoli, C. DeVault, E. Carnemolla, M. Ferrera, A. Boltasseva, V. M. Shalaev, D. Faccio, and M. Clerici, Broad frequency shift of parametric processes in epsilon-near-zero time-varying media, Applied Sciences **10**, 1318 (2020).
  - [10] K. Pang, M. Z. Alam, Y. Zhou, C. Liu, O. Reshef, K. Manukyan, M. Voegtle, A. Pennathur, C. Tseng, X. Su, *et al.*, Adiabatic frequency conversion using a time-varying epsilon-near-zero metasurface, Nano Letters **21**, 5907 (2021).
  - [11] R. Tirole, E. Galiffi, J. Dranczewski, T. Attavar, B. Tilmann, Y.-T. Wang, P. A. Huidobro, A. Alú, J. B.

- Pendry, S. A. Maier, *et al.*, Saturable time-varying mirror based on an epsilon-near-zero material, *Physical Review Applied* **18**, 054067 (2022).
- [12] D. Ramaccia, D. L. Sounas, A. Alù, F. Bilotti, and A. Toscano, Nonreciprocity in antenna radiation induced by space-time varying metamaterial cloaks, *IEEE Antennas and Wireless Propagation Letters* **17**, 1968 (2018).
- [13] A. Akbarzadeh, N. Chamanara, and C. Caloz, Inverse prism based on temporal discontinuity and spatial dispersion, *Optics letters* **43**, 3297 (2018).
- [14] M. Lyubarov, Y. Lumer, A. Dikopoltsev, E. Lustig, Y. Sharabi, and M. Segev, Amplified emission and lasing in photonic time crystals, *Science* **377**, 425 (2022).
- [15] R. Carminati, H. Chen, R. Pierrat, and B. Shapiro, Universal statistics of waves in a random time-varying medium, *Physical Review Letters* **127**, 094101 (2021).
- [16] E. Lustig, Y. Sharabi, and M. Segev, Topological aspects of photonic time crystals, *Optica* **5**, 1390 (2018).
- [17] A. Dikopoltsev, Y. Sharabi, M. Lyubarov, Y. Lumer, S. Tsesses, E. Lustig, I. Kaminer, and M. Segev, Light emission by free electrons in photonic time-crystals, *Proceedings of the National Academy of Sciences* **119**, e2119705119 (2022).
- [18] H. Li, S. Yin, H. He, J. Xu, A. Alù, and B. Shapiro, Stationary charge radiation in anisotropic photonic time crystals, *Physical Review Letters* **130**, 093803 (2023).
- [19] V. Bacot, M. Labousse, A. Eddi, M. Fink, and E. Fort, Time reversal and holography with spacetime transformations, *Nature Physics* **12**, 972 (2016).
- [20] V. Bacot, G. Durey, A. Eddi, M. Fink, and E. Fort, Phase-conjugate mirror for water waves driven by the faraday instability, *Proceedings of the National Academy of Sciences* **116**, 8809 (2019).
- [21] X. Zhu, H.-W. Wu, Y. Zhuo, Z. Liu, and J. Li, Effective medium for time-varying frequency-dispersive acoustic metamaterials, *Physical Review B* **108**, 104303 (2023).
- [22] E. Lustig, O. Segal, S. Saha, C. Fruhling, V. M. Shalaev, A. Boltasseva, and M. Segev, Photonic time-crystals-fundamental concepts, *Optics Express* **31**, 9165 (2023).
- [23] M. M. Asgari, P. Garg, X. Wang, M. S. Mirmoosa, C. Rockstuhl, and V. Asadchy, Photonic time crystals: Theory and applications, *arXiv preprint arXiv:2404.04899* (2024).
- [24] F. Wilczek, Quantum time crystals, *Physical review letters* **109**, 160401 (2012).
- [25] K. Kim, M.-S. Heo, K.-H. Lee, K. Jang, H.-R. Noh, D. Kim, and W. Jhe, Spontaneous symmetry breaking of population in a nonadiabatically driven atomic trap: an ising-class phase transition, *Physical review letters* **96**, 150601 (2006).
- [26] M.-S. Heo, Y. Kim, K. Kim, G. Moon, J. Lee, H.-R. Noh, M. Dykman, and W. Jhe, Ideal mean-field transition in a modulated cold atom system, *Physical Review E* **82**, 031134 (2010).
- [27] A. Shapere and F. Wilczek, Classical time crystals, *Physical review letters* **109**, 160402 (2012).
- [28] M. P. Zaletel, M. Lukin, C. Monroe, C. Nayak, F. Wilczek, and N. Y. Yao, Colloquium: Quantum and classical discrete time crystals, *Reviews of Modern Physics* **95**, 031001 (2023).
- [29] W. S. Edwards and S. Fauve, Patterns and quasi-patterns in the faraday experiment, *philosophical transactions of the royal society* **3**, 123 (1837).
- [30] T. B. Benjamin and F. J. Ursell, The stability of the plane free surface of a liquid in vertical periodic motion, *Proceedings of the Royal Society of London. Series A. Mathematical and Physical Sciences* **225**, 505 (1954).
- [31] W. S. Edwards and S. Fauve, Patterns and quasi-patterns in the faraday experiment, *Journal of Fluid Mechanics* **278**, 49 (1994).
- [32] N. Y. Yao, A. C. Potter, I.-D. Potirniche, and A. Vishwanath, Discrete time crystals: Rigidity, criticality, and realizations, *Physical review letters* **118**, 030401 (2017).
- [33] D. V. Else, C. Monroe, C. Nayak, and N. Y. Yao, Discrete time crystals, *Annual Review of Condensed Matter Physics* **11**, 467 (2020).
- [34] N. Basov, R. Ambartsumyan, V. Zuev, P. Kryukov, and V. Letokhov, Nonlinear amplification of light pulses, *Sov. Phys. JETP* **23**, 16 (1966).
- [35] S. V. Sazonov, Superluminal electromagnetic solitons in nonequilibrium media, *Physics-Uspekhi* **44**, 631 (2001).
- [36] Y. Pan, M.-I. Cohen, and M. Segev, Superluminal k-gap solitons in nonlinear photonic time crystals, *Physical Review Letters* **130**, 233801 (2023).
- [37] M.-I. Cohen, Y. Pan, O. Segal, and M. Segev, Annihilation of k-gap solitons in photonic time crystals, in *CLEO: Fundamental Science* (Optica Publishing Group, 2023) pp. FTu3D-6.
- [38] L. D. Landau and E. M. Lifshitz, *Mechanics* (Butterworth-Heinemann, 1976) ISBN 978-0750628969.
- [39] K. J. Burns, G. M. Vasil, J. S. Oishi, D. Lecoanet, and B. P. Brown, Dedalus: A flexible framework for numerical simulations with spectral methods, *Physical Review Research* **2**, 023068 (2020).
- [40] A. Altland and B. D. Simons, *Condensed matter field theory* (Cambridge university press, 2010).
- [41] H. W. Müller, Model equations for two-dimensional quasipatterns, *Physical Review E* **49**, 1273 (1994).
- [42] P. Chen and J. Vinals, Amplitude equation and pattern selection in faraday waves, *Physical Review E* **60**, 559 (1999).
- [43] V. E. Zakharov, V. S. L'vov, and S. S. Starobinets, Spin-wave turbulence beyond the parametric excitation threshold, *Soviet Physics Uspekhi* **17**, 896 (1975).

## SUPPLEMENTARY MATERIAL

### A. Expansion close to the instability threshold. Continuity of the phase transition.

Here, we explain the technical details involved in deriving the gradient descent dynamics of Eq. (9) in the near-critical regime. First, we reformulate the amplitude equations (4) in terms of the small parameter  $\epsilon = (h - h_c) / h_c = (\tilde{h} - \tilde{h}_c) / \tilde{h}_c$ :

$$\begin{aligned}\dot{\bar{a}} &= -\Omega\tilde{h}_c(2 + \epsilon)\bar{a} + \frac{\tilde{\beta}\Omega}{2}\bar{b}(\bar{a}^2 + \bar{b}^2) \\ \dot{\bar{b}} &= \Omega\tilde{h}_c\epsilon\bar{b} - \frac{\tilde{\beta}\Omega}{2}\bar{a}(\bar{a}^2 + \bar{b}^2).\end{aligned}\tag{S1}$$

The small  $\epsilon$  characterizes the growth of the unstable mode, which defines a slow time scale. We introduce an expansion in terms of  $\epsilon$ , such that  $\bar{a} = \epsilon^{1/4}\bar{a}_1 + \epsilon^{3/4}\bar{a}_2\dots$ ,  $\bar{b} = \epsilon^{1/4}\bar{b}_1 + \epsilon^{3/4}\bar{b}_2 + \dots$  and  $\partial_t = \partial_{t_0} + \epsilon\partial_{t_1}$ . At orders  $\epsilon^{1/4}$  and  $\epsilon^{3/4}$ , we obtain

$$\begin{aligned}\frac{\partial\bar{a}_1}{\partial t_0} &= -2\Omega\tilde{h}_c\bar{a}_1 \\ \frac{\partial\bar{a}_2}{\partial t_0} &= -2\Omega\tilde{h}_c\bar{a}_2 - \frac{\tilde{\beta}\Omega}{2}\bar{b}_1(\bar{a}_1^2 + \bar{b}_1^2).\end{aligned}$$

These equations describe a quick relaxation towards the fixed point

$$\begin{aligned}\bar{a}_1 &= 0 \\ \bar{a}_2 &= -\frac{\tilde{\beta}}{4\tilde{h}_c}\bar{b}_1^3.\end{aligned}\tag{S2}$$

At order  $\epsilon^{5/4}$ , we derive the equation

$$\frac{\partial\bar{b}_1}{\partial t_1} = \tilde{h}_c\Omega\bar{b}_1 + \frac{\tilde{\beta}\Omega}{2}\bar{a}_2\bar{b}_1^2.$$

For a small  $\epsilon$ , we can assume that the relaxation of  $\bar{a}_2$  towards the value given in Eq. (S2) is infinitely fast, and write

$$\frac{\partial\bar{b}_1}{\partial t_1} = \tilde{h}_c\Omega\bar{b}_1 - \frac{\tilde{\beta}^2\Omega}{8\tilde{h}_c}\bar{b}_1^5.\tag{S3}$$

Restoring the original variables  $t$  and  $\bar{b}$  we obtain

$$\frac{\partial\bar{b}}{\partial t} = \epsilon\tilde{h}_c\Omega\bar{b} - \frac{\tilde{\beta}^2\Omega}{8\tilde{h}_c}\bar{b}^5.$$

This is the gradient descent dynamics described by Eq. (9) of the main text.

### B. Goldstone-like Modes

We add a time and space dependent phase to the steady state solution found in the main text for low damping:

$$D_\phi(x, t) = \pm\sqrt{\frac{8h}{9\beta}}\sin(\Omega t)\cos(q^*x + \phi(x, t)).\tag{S4}$$

Here,  $\phi(x, t_0) \ll 1$ . We seek to derive an equation governing the dynamics of the phase  $\phi(x, t)$ . To this purpose, we write

$$\begin{aligned}D_\phi(x, t_0) &= \frac{A}{2}\sin(\Omega t - qx - \phi(t, x)) \\ &\quad + \frac{A}{2}\sin(\Omega t + qx + \phi(t, x)),\end{aligned}\tag{S5}$$

where  $A = \sqrt{8h/9\beta}$ . In what follows, we will use the abbreviations  $\sin(\Omega t - qx - \phi(t, x)) = \sin(-)$  and  $\sin(\Omega t + qx + \phi(t, x)) = \sin(+)$  and similar for cos-terms. Inserting Eq. (S5) into Eq. (1) and comparing the coefficients in front of the cos (+) terms we find an equation for  $\phi(t, x)$ :

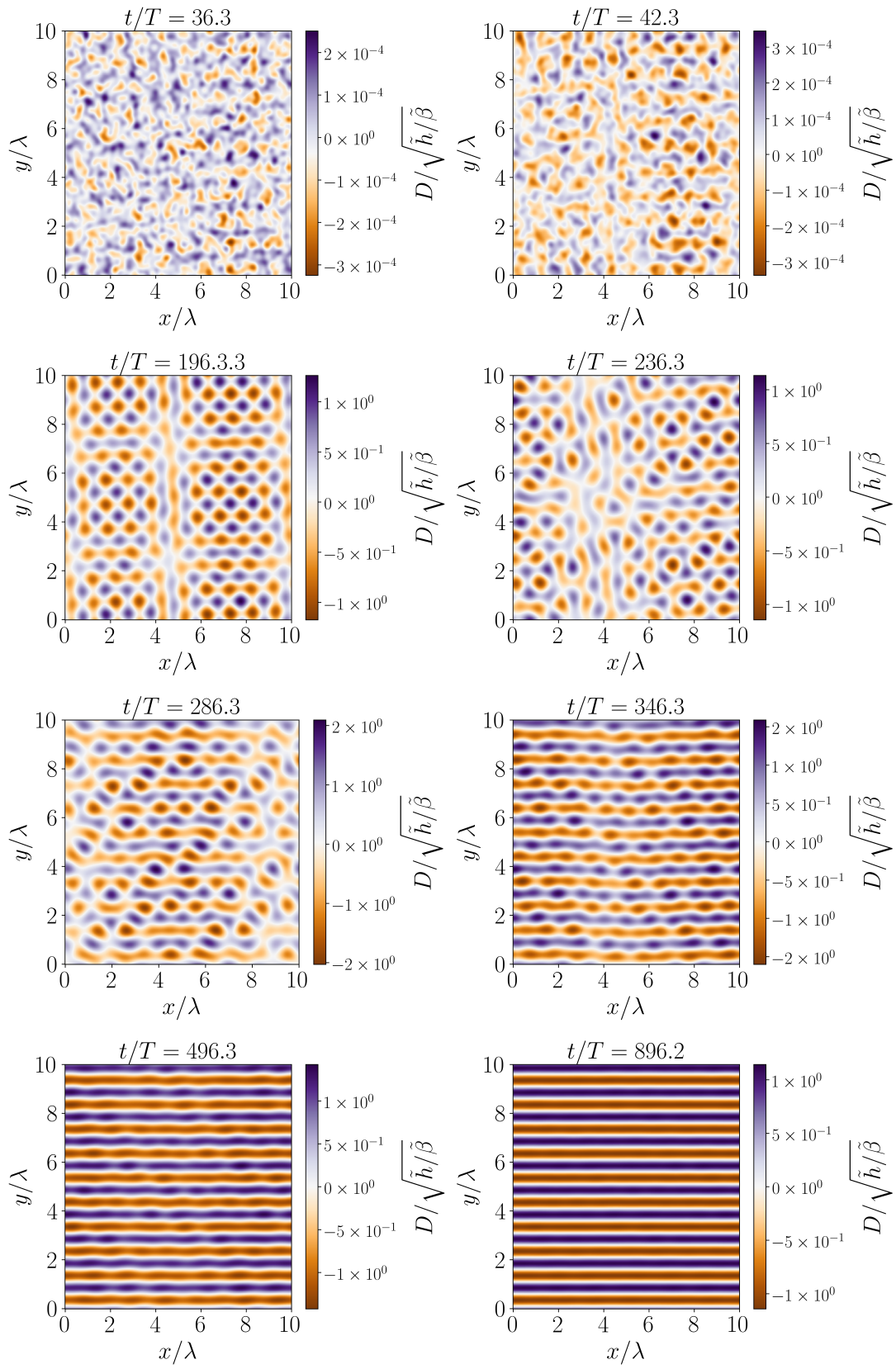
$$\frac{1}{c^2} \frac{\partial^2 \phi}{\partial t^2} = \left(1 - \frac{1}{3}h\right) \frac{\partial^2 \phi}{\partial x^2}. \quad (\text{S6})$$

The same equation follows from the cos (-) terms. The sin ( $\pm$ ) terms, on the other hand, give corrections of order  $Q/q^*$  to the solution (S4). These can be neglected for a smooth, small- $Q$  perturbation of the kind that we are considering. Compared to the velocity of electromagnetic waves in the undriven medium, the velocity of the Goldstone mode  $c_G$  is reduced by a factor that depends on the amplitude of the time varying term in Eq. (1):

$$c_G = \sqrt{1 - \frac{1}{3}hc}.$$

### C. Pattern formation in two dimensions





Supplementary Figure S 1. Pattern formation in a two-dimensional PTC.